


RESEARCH

Open Access



# Weipiling decoction alleviates *N*-methyl-*N*-nitro-*N'*-nitrosoguanidine-induced gastric precancerous lesions via NF- $\kappa$ B signalling pathway inhibition

Penghui Yang<sup>1</sup>, Hongmei Yang<sup>1,2</sup>, Hengli Zhou<sup>1</sup>, Qiuyue Li<sup>1</sup>, Sufen Wei<sup>3</sup>, Qi Wang<sup>1</sup>, Yan Yan<sup>4</sup>, Yongqiang Liu<sup>5</sup>, Huafeng Pan<sup>1\*</sup> and Siyi Li<sup>6,7,8\*</sup> 

## Abstract

**Aim of the study:** We aimed to explore how weipiling (WPL) decoction WPL alleviates gastric precancerous lesions (GPLs) and uncover its anti-inflammatory roles in GPL treatment.

**Materials and methods:** The anti-GPL action mechanisms of WPL were analysed using a network pharmacological method. The WPL extract was prepared in a traditional way and evaluated for its major components using high-performance liquid chromatography with tandem mass spectrometry (HPLC–MS/MS). BALB/c mice were exposed to *N*-methyl-*N*-nitro-*N'*-nitrosoguanidine (MNNG) (150  $\mu$ g/mL) for 6 weeks to induce GPLs. GPL mice were administered WPL (3.75 g/kg/day and 15 g/kg/day) for an additional 8 weeks. Haematoxylin and eosin (H&E) staining was used to investigate histological alterations in gastric tissues. Expression of the T helper 1 (Th1) cell markers CD4<sup>+</sup> and interferon-gamma (INF- $\gamma$ ) were tested using immunohistochemistry (IHC). Inflammatory protein and mRNA levels in the nuclear factor kappa B (NF- $\kappa$ B) pathway were detected using western blotting and a quantitative reverse transcription polymerase chain reaction (RT-qPCR), respectively.

**Results:** We identified and selected 110 active compounds and 146 targets from public databases and references. Four representative components of WPL were established and quantified by HPLC–MS/MS analysis. WPL attenuated MNNG-induced GPLs, including epithelial shedding, cavity fusion, basement membranes with asymmetrical thickness, intestinal metaplasia, dysplasia, pro-inflammatory Th1-cell infiltration, and INF- $\gamma$  production, indicating that WPL prevents inflammation in the gastric mucosa. Furthermore, WPL reversed MNNG-induced activation of the I $\kappa$ B/NF- $\kappa$ B signalling pathway and subsequently attenuated the upregulation of inducible nitric oxide synthase (iNOS), cyclooxygenase-2 (COX-2), and nicotinamide adenine dinucleotide phosphate oxidase (NADPH oxidase (NOX)) family members NOX2 and NOX4.

**Conclusion:** WPL attenuated GPLs by controlling the generation of pro-inflammatory elements and inhibiting the NF- $\kappa$ B signalling pathway in vivo.

\*Correspondence: gzphf@gzucm.edu.cn; lisiyi@gzucm.edu.cn

<sup>1</sup> Science and Technology Innovation Center, Guangzhou University of Chinese Medicine, Guangzhou 510405, China

<sup>8</sup> Dongguan Institute of Guangzhou University of Chinese Medicine, Dongguan 523808, China

Full list of author information is available at the end of the article



© The Author(s) 2022. **Open Access** This article is licensed under a Creative Commons Attribution 4.0 International License, which permits use, sharing, adaptation, distribution and reproduction in any medium or format, as long as you give appropriate credit to the original author(s) and the source, provide a link to the Creative Commons licence, and indicate if changes were made. The images or other third party material in this article are included in the article's Creative Commons licence, unless indicated otherwise in a credit line to the material. If material is not included in the article's Creative Commons licence and your intended use is not permitted by statutory regulation or exceeds the permitted use, you will need to obtain permission directly from the copyright holder. To view a copy of this licence, visit <http://creativecommons.org/licenses/by/4.0/>. The Creative Commons Public Domain Dedication waiver (<http://creativecommons.org/publicdomain/zero/1.0/>) applies to the data made available in this article, unless otherwise stated in a credit line to the data.

**Keywords:** Weipiling decoction, Gastric precancerous lesion, NF- $\kappa$ B, *N*-methyl-*N*-nitro-*N*-nitrosoguanidine, Inflammation

## Introduction

Gastric cancer (GC) is a prevalent and fatal global malignancy [1, 2], and its incidence and mortality rates are still high in China [3]. Reportedly, approximately 26,380 new GC cases and 11,090 GC deaths in the U.S. in 2022 [4]. Surgery and chemotherapy are the main GC treatment strategies. However, most patients with GC benefit poorly from current treatments because they are usually diagnosed at advanced stages [5]. Therefore, early diagnosis and treatment are recognised as effective strategies to reduce GC mortality. To date, gastric precancerous lesions (GPLs), including chronic atrophic gastritis (CAG), dysplasia, and intestinal metaplasia (IM), are progressive stages prior to tumorigenesis in the gastric mucosa [6]. Moreover, it can prevent and reverse GPL progression via rational early treatment [7, 8]. Therefore, diagnostic and therapeutic management of GPLs is a critical strategy to reduce GC mortality.

GPLs are recognized as a chronic inflammatory state of the gastric mucosa. GPLs endure malignant transformation through long-term exposure to pro-inflammatory stimuli [9, 10], such as dietary patterns, obesity, smoking, and chronic infections [11]. One of the most common GPL stimuli is *N*-nitroso compounds (NOCs), which are frequently found in salted vegetables, fish, meat, and other salted foods [12]. NOCs chronically induce gastric carcinogenesis by promoting a pro-inflammatory response and stimulating DNA damage in the gastric mucosa [13, 14]. Therefore, *N*-methyl-*N*-nitro-*N*-nitrosoguanidine (MNNG), a carcinogenic NOC, is widely used to mimic GPLs in mice because of its DNA-damaging properties [11, 15–17] and inflammation-induced metaplasia in acid-secreting parietal cells [18]. Thus,

MNNG-induced GPLs are a rational model to investigate the pathogenesis of gastric mucosa GPLs and inflammation.

Weipiling (WPL) decoction, a derivative of the Sijunzi decoction formula in ancient Chinese medicine, has been used to treat gastric disease and prevent GC for centuries in China. One significant symptom of GPL patients is summarised as “Qi deficiency” according to Chinese medicine theory and clinical practice. The WPL formula is frequently used to treat GPLs and prevent GC transfer due to its “Qi-refuelling” property. To date, WPL is still commonly prescribed to GPL patients in Chinese medicine hospitals [19], but its GPL-alleviating mechanism remains elusive. The composition of WPL, including *Astragalus mongholicus* Bunge (Huang Qi), *Atractylodes lancea* (Thunb.) DC (Bai Zhu), *Poria cocos* (Schw.) wolf (Fu Ling), *Pseudostellaria heterophylla* (Miq.) Pax (Tai Zi Shen), *Panax notoginseng* (Burkill) F. H. Chen (San Qi), *Scleromitron diffusum* (Willd.) R. J. Wang (Bai Hua She Cao), *Curcuma zedoaria* (Christm.), *Roscoe* (E zhu), *Heridium erinaceus* (Bull.), and *Pers* (Hou Gu Jun) (Table 1), exerts potential GPL-alleviating and nuclear factor kappa B (NF- $\kappa$ B)-related anti-inflammatory activities. *Heridium erinaceus* (Bull.) *Pers* is critical in treating inflammatory diseases. Compounds extracted from *Atractylodes lancea* (Thunb.) DC, such as beta-eucalyptol and atractylone, inhibit inflammation by blocking the NF- $\kappa$ B signalling pathway [20–22]. A previous study also found that the main components of WPL, *Scleromitron diffusum* (Willd.) R. J. Wang and *Heridium erinaceus* (Bull.) *Pers*, are used to treat gastrointestinal diseases, such as GC and CAG by attenuating tumour angiogenesis and proliferation

**Table 1** Components and ratio of WPL

Local name	English name	Used part	Percentage (%)
Huang Qi	<i>Astragalus mongholicus</i> Bunge	Root	20
Bai Zhu	<i>Atractylodes lancea</i> (Thunb.) DC	Root	10
E Zhu	<i>Curcuma zedoaria</i> (Christm.), <i>Roscoe</i>	Root	9
Fu Ling	<i>Poria cocos</i> (Schw.) wolf	Sclerotium	10
Tai Zi Shen	<i>Pseudostellaria heterophylla</i> (Miq.) Pax	Root	10
San Qi	<i>Panax notoginseng</i> (Burkill) F. H. Chen	Root	5
Bai Hua She She Cao	<i>Scleromitron diffusum</i> (Willd.) R. J. Wang	Grass	15
Hou Gu Jun	<i>Heridium erinaceus</i> (Bull.) <i>Pers</i>	Sclerotium	16
Shou Gong	<i>Gecko</i>	Total	5

and inducing apoptosis [23–31]. The major chemical components of WPL, including notoginsenoside R1, calycosin-7-*O*-beta-*D*-glucoside, astragaloside A, and adenine-9- $\beta$ -*D*-ribofuranoside, were determined using high-performance liquid chromatography with tandem mass spectrometry (HPLC–MS/MS). However, the anti-inflammatory potential of WPL in GPLs remains unclear.

Network pharmacology approaches, including cheminformatics, bioinformatics, network biology and pharmacology, are effective methods to study and elucidate the mechanisms of drug action [32]. In this research, we used network pharmacological analysis to illustrate the action mechanisms of WPL improving GPLs. Molecular docking was used to verify the binding ability of active compounds and potential targets in WPL. We constructed an MNNG-induced mouse model and attested the anti-inflammatory effect of WPL in *in vivo* experiments.

## Materials and methods

### Collecting WPL active ingredients and targets

The active ingredients were obtained from the Traditional Chinese Medicine Integrated Database (TCMID, <http://www.megabionet.org/tcmid/>) [33] and Traditional Chinese Medicine Systems Pharmacology Database and Analysis Platform (TCMSP, <http://sm.nwsuaf.edu.cn/lsp/tcmsp.php>) [34]. However, the active ingredients of *Hericium erinaceus* (Bull.) Pers and *Gecko* were not found in the TCMID or TCMSP. WPL-related targets were retrieved from TCMID, TCMSP, and the Search Tool for Interacting Chemicals (STITCH, <http://stitch.embl.de>) [35], then screened with a medium compound-target association score greater than 400 in the STITCH database. The target information was standardised using NCBI (<https://www.ncbi.nlm.nih.gov/>). Next, a drug-like analysis of WPL active components was carried out according to the quantitative estimate of drug-likeness (QED) proposed by Bickerton [36] with a QED  $\geq$  0.3. Subsequently, WPL active compounds and targets were screened using a binomial statistical model [37].

We searched for *Hericium erinaceus* (Bull.) Pers active components and targets in Herb Ingredients' Targets (HIT, <http://lifecenter.sgst.cn/hit/>) and deleted some active constituents with no targets [38]. Additionally, calycosin 7-*O*-glucoside and notoginsenoside R1 targets, which have high drug activities, were retrieved from the PharmMapper (<http://www.lilab-ecust.cn/pharmmapper>) platform with a median Norm Fit  $\geq$  0.6008 and 0.4921, respectively, followed by further searches with a median Norm Fit  $\geq$  0.72915 and 0.586, respectively.

### Collecting GPL targets

GPL targets were collected from the GeneCards (<https://www.genecards.org>) database with “gastric precancerous lesions” as the search words, then screened with relevance scores  $\geq$  5.

### Protein–protein interaction (PPI) network construction

The PPI network was constructed using the STRING database (<https://cn.string-db.org/>) using common targets obtained from GPL cure targets and WPL-related targets using the Venny 2.1 tool. The PPI network was visualised using Cytoscape software 3.8.0.

### Function enrichment analysis

Gene Ontology (GO) and Kyoto Encyclopaedia of Genes and Genomes (KEGG) pathway enrichment analyses were performed using the clusterProfiler package 3.15.4. A significant enrichment analysis was set at  $P \leq$  0.01.

### Molecular docking analysis

Zinc (<http://zinc15.docking.org>) [39] and the Protein Data Bank (PDB, <http://www.rcsb.org/pdb/>) [40] were used to download the chemical structure of compounds and the three-dimensional structure of targets, respectively. Molecular docking analysis was performed using AutoDock Vina 1.1.2 [41] and plotted using PyMol 2.3.0 [42].

### Reagents and antibodies

Methanol, acetonitrile, and HPLC-grade acetic acid were purchased from Merck (Darmstadt, Germany). The reference substances *notoginsenoside R1*, *calycosin-7-*O*-beta-*D*-glucoside*, *astragaloside A*, and *adenine-9- $\beta$ -*D*-ribofuranoside*, with HPLC-verified purities >98%, and vitamin B12 (VitB12) were obtained from Meilun Biotechnology Co., Ltd. (Dalian, China). MNNG was provided by the Tokyo Chemical Industry (TCI) (Tokyo, Japan). Primary antibodies against inducible nitric oxide synthase (iNOS, Abcam, Cambridge, MA, USA, ab178945), cyclooxygenase-2 (COX-2, Abcam, ab179800), NOX-2 (Abcam, ab129068), NOX-4 (Abcam, ab154244), NF- $\kappa$ B p65 (8242S, Cell Signalling Technology (CST), Beverly, MA, USA), phospho-NF- $\kappa$ B p65 (CST, 3033S), I $\kappa$ B- $\alpha$  (CST, 4814S), phospho-I $\kappa$ B- $\alpha$  (CST, 2859S), CD4<sup>+</sup> (CST, 93518S), interferon-gamma (IFN- $\gamma$ , CST, 8455S), and glyceraldehyde 3-phosphate dehydrogenase (GAPDH, CST, 5174S) () were used for western

blotting or immunohistochemistry (IHC). The secondary horseradish peroxidase (HRP)-conjugated antibody (8114S) was from CST. All other reagents and chemicals used in this study were of analytical grade.

#### Preparing and phytochemically analysing WPL

WPL consists of nine herbs: Huang Qi (Guangdong Tiancheng Prepared Herbal Medicine Co., Ltd., China, 200501), Bai Zhu (Guangdong Zhixin traditional Chinese medicine Tabl Co., Ltd., China, 201101), Fu Ling (Guangdong Zhixin traditional Chinese medicine Tabl Co., Ltd., 201002), E Zhu (Guangdong medicinal materials co., China, E0520011), Tai Zi Shen (Guangdong medicinal materials co., T3520011), San Qi (KANGMEI, China, 201201201), Bai Hua She Cao (Guangdong medicinal materials co., B2020912), and Hou Gu Jun (Guangzhou Ziyunxuan Pharmaceutical Co., Ltd., China, 201001) Voucher specimens were deposited at the School of Pharmaceutical Sciences, Guangzhou University of Chinese Medicine (Guangzhou, China). All these herbs were extracted in water ten times the amount of the herbs and boiled twice for 2 h each. Next, San Qi and Hou Gu Jun powders were added and mixed. It was uniformly concentrated at 60 °C under reduced pressure, then vacuum-dried, and crushed to obtain 1 g of extract equivalent to 3.33 g of the crude drug. For in vivo management, WPL was dissolved in water (450 mg/mL).

WPL was dissolved in methanol (10 mg/mL), and a 5- $\mu$ m filter or WPL solution was filtered by HPLC–MS/MS analysis to phytochemically examine the WPL components.

WPL was characterised using the negative and positive ionisation modes of TSQ Quantum Ultra-EMR HPLC–MS/MS (Thermo Scientific, USA). The operating parameters were as follows: an ion source applying ESI and an ion spray voltage of 3000 V in both positive and negative modes. For two modes, the low rate of sheath gas and the low rate of auxiliary gas were 30 mL/min and 10 mL/min, respectively, and the probe heater and capillary temperatures were set at 350 °C and 300 °C, respectively. The skimmer level was set to 1. Parallel reaction monitoring (PRM) scanning was performed to obtain MS data at a resolution of 70,000. Additionally, sample analyses were

performed at 9, 17, and 18 normalised collision energies (NCE), and the MS detection resolution was 17,500. The TSQ Tune software Trace Finder (Thermo Scientific) was used to set up the instrument and process the quantitative data.

HPLC analysis was conducted on a Phenomenex C18 column (50 mm  $\times$  2.1 mm, 5  $\mu$ m) with mobile phases A (acetonitrile) and B (0.1% formic acid) (v/v). The flow velocity was set to 1 mL/min, and the injection volume was 5  $\mu$ L. A linear gradient (initial 0% A, 5% A 0–0.5 min; 5–95% A 0.5–1 min; 95% A 1.0–2.5 min; 95–5% A 2.5–3 min) was used for elution. The retention duration and HPLC–MS/MS data of WPL extracts and the reference compounds were compared to identify compounds, including notoginsenoside R1, calycosin-7-O-beta-D-glucoside, astragaloside A, and adenine-9- $\beta$ -D-ribofuranoside.

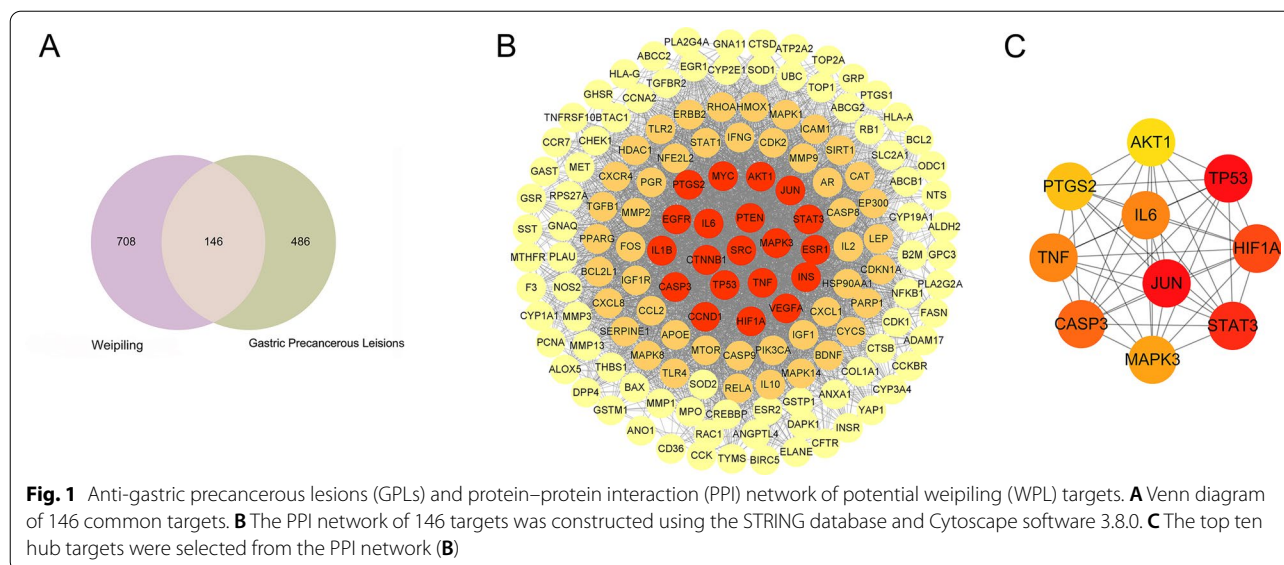
Quantitative determination was performed by using six-point regression curves. Four reference compounds were used to prepare a stock solution diluted with methanol to a suitable concentration. HPLC–MS/MS was conducted to analyse the standard and WPL solutions. The peak area of each reference compound was calculated from the calibration curves. Compound contents in WPL were expressed as mg/g and was calculated after the correlation between the peak area and the calibration curves of each analyte (Table 2).

#### Animal experiments

Male BALB/c mice (2-month-old, 18–22 g) were purchased from the Laboratory Animal Centre of the Guangzhou University of Chinese Medicine. All mice were maintained at 23  $\pm$  1 °C with sufficient water and food. The mice were randomly divided into five groups (n = 10 per group): vehicle control (H<sub>2</sub>O), MNNG (150  $\mu$ g/mL), MNNG + WPL (3.75 g/kg/day and 15 g/kg/day), and MNNG + VitB12 (1 mg/kg). VitB12 was applied as the positive control for GPLs. The mice were administered an MNNG solution (150  $\mu$ g/mL) with free drinking water for 6 weeks. After constructing the GPL mouse model by administering MNNG for 6 weeks, the respective groups orally received equal volumes of WPL, VitB12, or the vehicle for 8 weeks. The mice were sacrificed after the last

**Table 2** Quantitatively determined parameters of reference compounds in WPL

Analyte	Linearity range ( $\mu$ g/mL)	Regression equation $Y = ax + b$	$r^2$
Notoginsenoside R1	0.000475–0.95	$y = 11.58x - 1.269$	0.9997
Adenine-9- $\beta$ -D-ribofuranoside	0.422–13.5	$y = 9.28E4x + 39.8$	0.9994
Astragaloside A	22.82–456.3	$y = 1.74E5x - 1.10E3$	0.9999
Calycosin-7-O-beta-D-glucoside	4.00–120.0	$y = 2.84E7x - 1.505E5$	0.9995



administration, and stomach tissues were collected for further experiments. MNNG was dissolved in H<sub>2</sub>O to a concentration of 2 mg/mL and stored at 4 °C in the dark. This study was approved by the Institutional Animal Care and Use Committee of Guangzhou University of Traditional Chinese Medicine (NO.20201028003).

#### Histological examination

The stomach tissues were fixed with 4% PFA in 0.1 mol/L phosphate buffer overnight, embedded in paraffin, and cut into 4- $\mu$ m slices. Standard techniques were used to stain the sections with haematoxylin and eosin (H&E) to observe histological changes.

#### Immunohistochemistry

Formalin-fixed, paraffin-embedded gastric mucosal tissues were selected to perform IHC. Sections were deparaffinized and rehydrated with xylene and graded ethanol to water, followed by antigen retrieval and tissue blocking using 3% normal non-immune serum. Next, they were incubated with the primary antibodies IFN- $\gamma$  (Abcam, ab9657, rabbit, polyclonal, 1/400) and CD4 (Abcam, ab203034, rabbit, polyclonal, 1/200) per the kit protocol (KGOS60, KeyGEN, Nanjing, China) at 4 °C overnight. After being washed with phosphate-buffered saline (PBS), the sections were incubated with HRP-conjugated secondary antibodies for 30 min at an ambient temperature. Tissue sections were stained with 3,3'-diaminobenzidine (DAB) and haematoxylin. The IHC results were observed under a microscope and analysed using Image-Pro Plus software (version 6.0; Media Cybernetics, Silver Spring, MD, USA) with the average

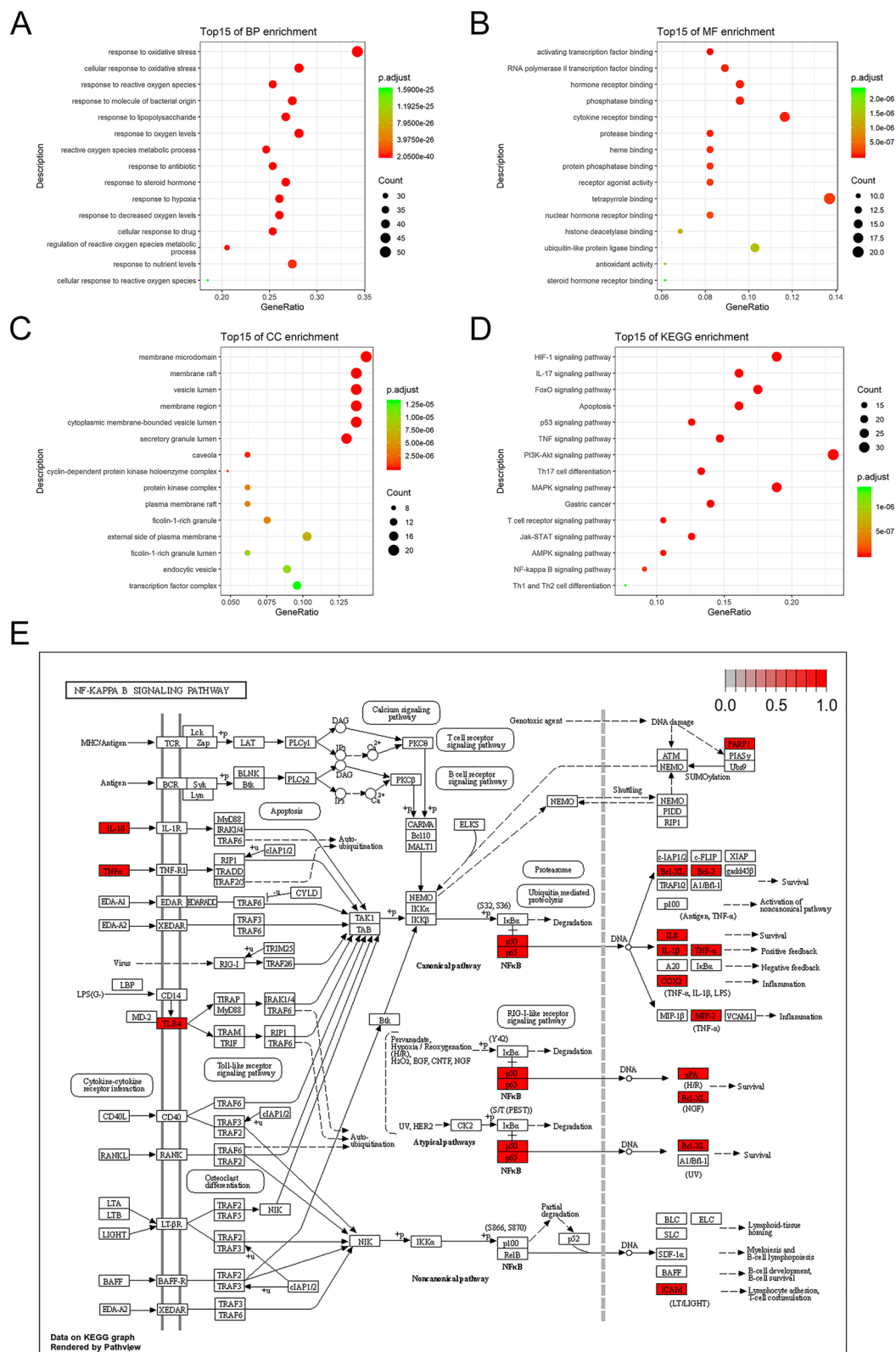
combined optical density (IOD) to positive part (IOD/pixel) ratios.

#### Western blotting

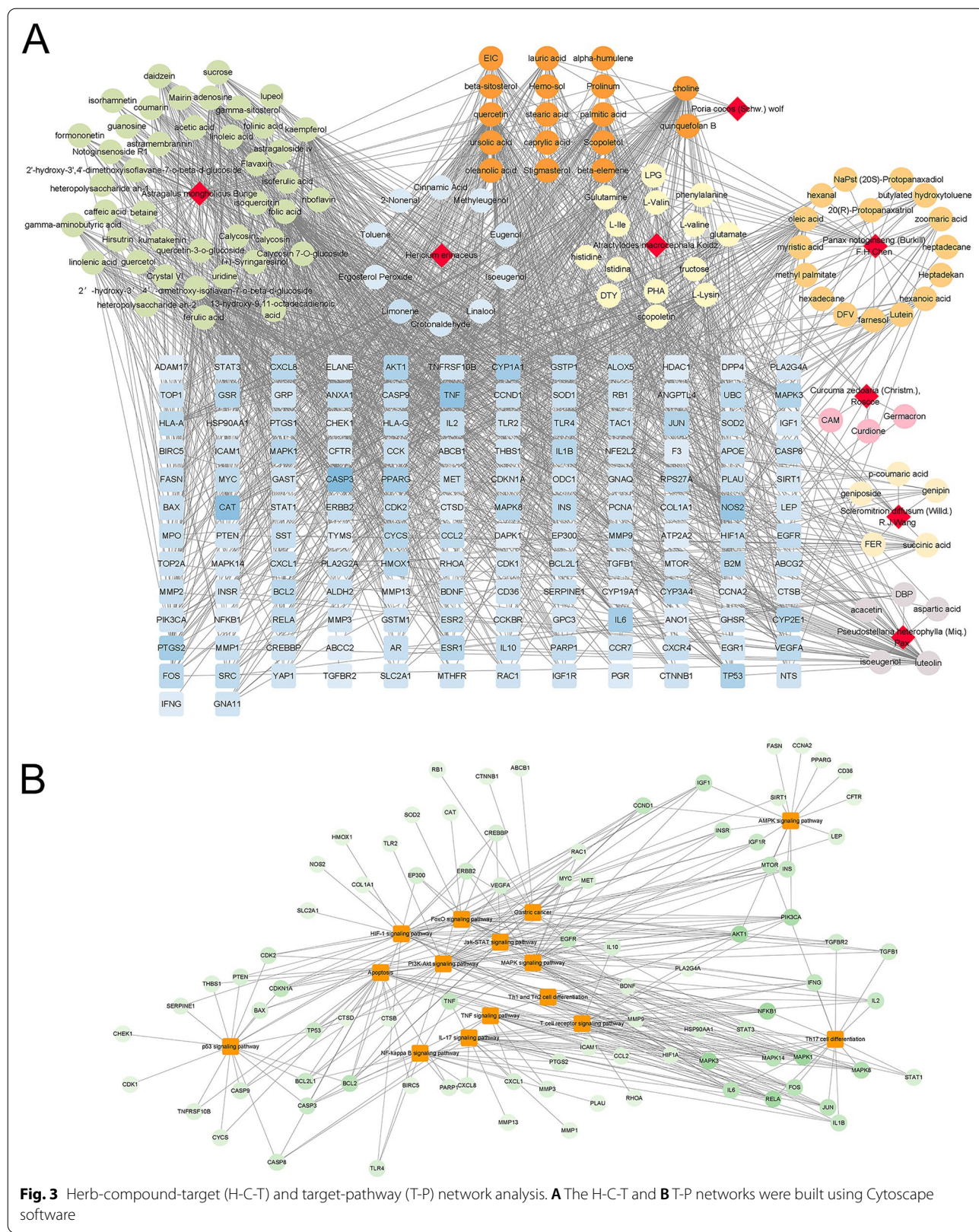
After preparation with radioimmunoprecipitation assay (RIPA) lysis buffer, protein samples were quantitated using a bicinchoninic acid (BCA) protein assay. Equal amounts of proteins were separated by sodium dodecyl-sulphate polyacrylamide gel electrophoresis (SDS-PAGE), transferred to polyvinylidene fluoride (PVDF) membranes which were blocked with 5% bovine serum albumin (BSA) solution, and incubated with primary antibodies at 4 °C overnight. The next day, the membrane was rinsed with Tris-buffered saline and Tween 20 (TBST), followed by incubation with HRP-conjugated secondary antibodies for 2 h at room temperature. Protein levels were detected using a chemiluminescence assay kit (Millipore, Massachusetts, USA). The density analysis of immunoblots was conducted using ImageJ software (NIH, USA).

#### Quantitative reverse transcription PCR (RT-qPCR)

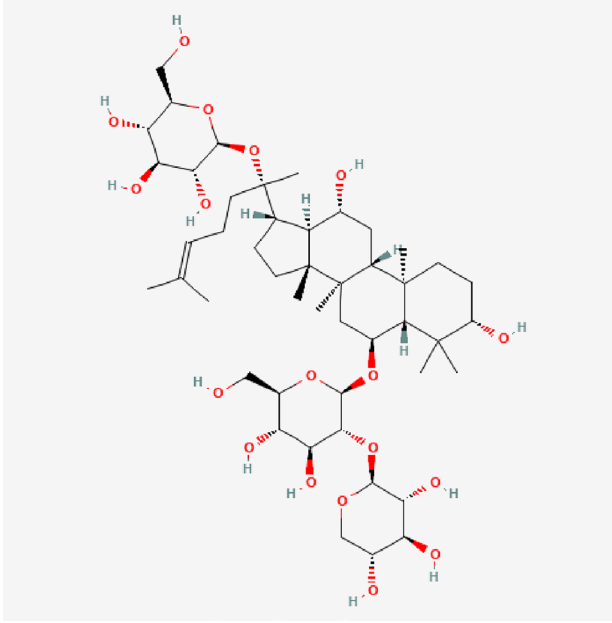
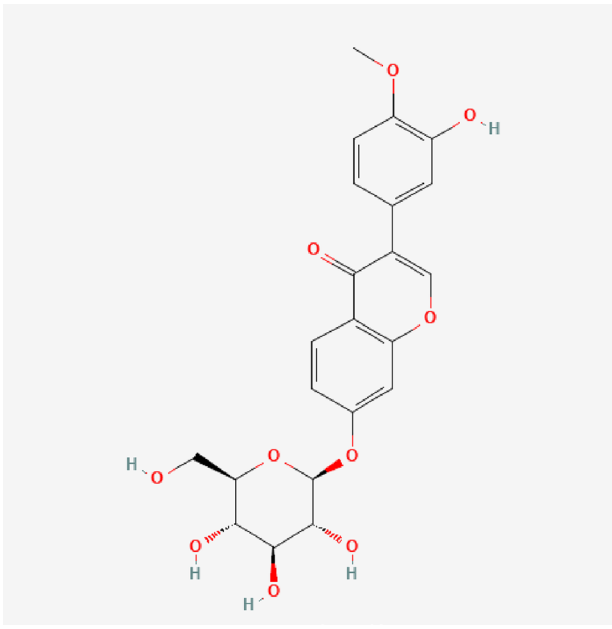
Total RNA was isolated from gastric mucosal tissues using a TRIzol reagent. Per the manufacturer's protocol, we used the One-Step PrimeScript RT-PCR Kit to synthesise complementary DNA (cDNA) from total RNA. Next, qPCR was performed using ChamQTM Universal SYBR qPCR Master Mix (the reagents above were obtained from Vazyme Biotech Co., Ltd., Nanjing, China) and analysed on an ABI 7500 sequence detection system. The experiments were performed in triplicate, and the primer sequences were as follows: tumour necrosis factor



**Fig. 2** Gene Ontology (GO) and Kyoto Encyclopedia of Genes and Genomes (KEGG) enrichment analyses. **A** Top 15 biological process (BP) enrichment items. **B** Top 15 molecular function (MF) enrichment items. **C** Top 15 cellular components (CC) enrichment items. **D** Top 15 KEGG enrichment items. **E** Map of the NF-κB signalling pathway. Red boxes represent the key targets

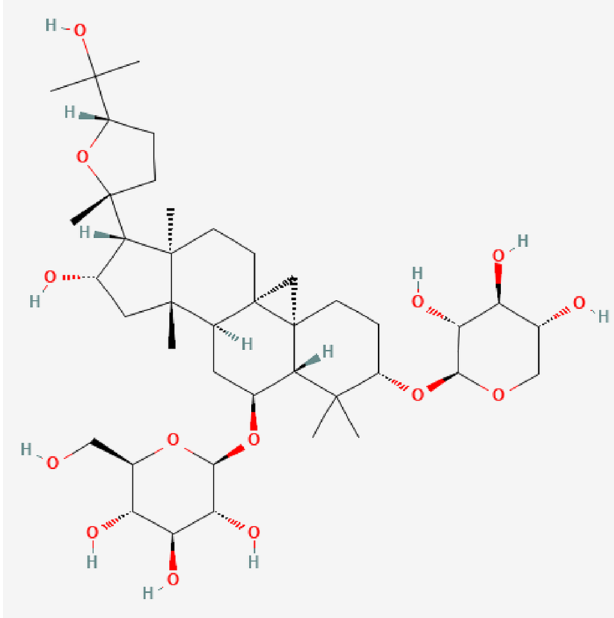
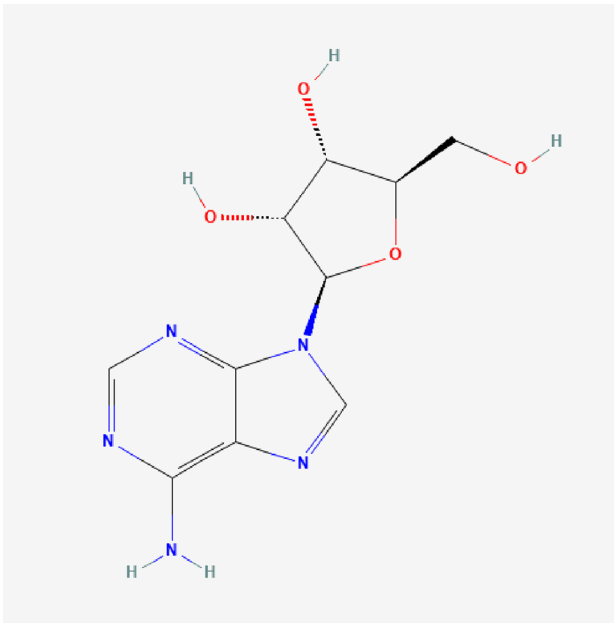


**Table 3** Chemical structures of WPL active compounds

Synonyms	Cas	Molecular Formula	2D Structure
Notoginsenoside R1	80418-24-2	C <sub>47</sub> H <sub>80</sub> O <sub>18</sub>	 The image shows the chemical structure of Notoginsenoside R1, a complex triterpenoid saponin. It features a central pentacyclic triterpene core with multiple methyl groups and a side chain containing a double bond. This core is linked via an ether bridge to a glucose molecule, which is further linked to another glucose molecule at the C-6 position. The structure is shown in a 2D perspective with stereochemistry indicated by wedges and dashes.
Calycosin-7-O-β-D-glucoside	20633-67-4	C <sub>22</sub> H <sub>22</sub> O <sub>10</sub>	 The image shows the chemical structure of Calycosin-7-O-β-D-glucoside. It consists of a calycosin aglycone, which is a flavone with a methoxy group at the 5-position and a hydroxyl group at the 7-position. The 7-hydroxyl group is linked to a glucose molecule at the C-7 position. The structure is shown in a 2D perspective with stereochemistry indicated by wedges and dashes.



**Table 3** (continued)

Synonyms	Cas	Molecular Formula	2D Structure
Astragaloside IV	84687-43-4	C <sub>41</sub> H <sub>68</sub> O <sub>14</sub>	
Quinquefolan B	109767-06-8	C <sub>10</sub> H <sub>13</sub> N <sub>5</sub> O <sub>4</sub>	

alpha (TNF- $\alpha$ ), forward 5'-AGGGTCTGGGC CATAGA ACT-3' and reverse 5'-CCACCACGCTCTTCTGTC TAC-3'; interleukin (IL)-6 (IL-6), forward 5'-ATGATG AGAAACGAGCCAATTG-3' and reverse 5'-GCTTTG GCTTCTTTCTTACGAG-3'.

**Statistical analysis**

All quantitative measures are described as the average  $\pm$  standard deviation (SD). Two independent groups were compared using an unpaired *t*-test. Differences between more than two groups were compared using

**Table 4** Molecular docking results

Chem	GENE	PDB	Best affinity
Calycosin-7-O-β-D-glucoside	MAPK3	4qtb	- 9.1
Astragaloside IV	JUN	1s9k	- 8.7
Notoginsenoside R1	JUN	1s9k	- 8.2
Notoginsenoside R1	NOS2	3e7g	- 8.2
Astragaloside IV	TNF	2az5	- 8.2
Notoginsenoside R1	TNF	2az5	- 8
Calycosin-7-O-β-D-glucoside	NOS2	3e7g	- 7.9
Astragaloside IV	MAPK3	4qtb	- 7.7
Astragaloside IV	NOS2	3e7g	- 7.7
Calycosin-7-O-β-D-glucoside	JUN	1s9k	- 7.5
Notoginsenoside R1	BCL2	2w3l	- 7.2
Notoginsenoside R1	TP53	3q05	- 7.1
Quinquefolan B	MAPK3	4qtb	- 7.1
Calycosin-7-O-β-D-glucoside	CASP3	1gfw	- 7.1
Astragaloside IV	CASP3	1gfw	- 7.1
Quinquefolan B	NOS2	3e7g	- 6.9
Calycosin-7-O-β-D-glucoside	TP53	3q05	- 6.9
Quinquefolan B	TNF	2az5	- 6.8
Astragaloside IV	TP53	3q05	- 6.7
Astragaloside IV	BCL2	2w3l	- 6.7
Notoginsenoside R1	CASP3	1gfw	- 6.6
Calycosin-7-O-β-D-glucoside	TNF	2az5	- 6.6
Quinquefolan B	JUN	1s9k	- 6.4
Calycosin-7-O-β-D-glucoside	BCL2	2w3l	- 6.3
Quinquefolan B	CASP3	1gfw	- 6.1
Notoginsenoside R1	MAPK3	4qtb	- 6
Quinquefolan B	TP53	3q05	- 5.4

a one-way analysis of variance (ANOVA), followed by Dunnett's post-hoc test.  $P < 0.05$  was regarded as statistically significant. All data analyses were performed using GraphPad Prism 7.0 (GraphPad Software, San Diego, CA, USA). All experiments were conducted in triplicates.

## Results

### Screened WPL active compound and GPL targets

We obtained 282 active compounds and 6767 targets of WPL from the public databases. Based on a QED  $\geq 0.3$ , 150 active compounds were identified. In addition, 127 active compounds and 758 targets were identified using a binomial statistical model. Additionally, 12 compounds and 43 targets of *Hericium erinaceus* (Bull.) Pers were retrieved from the HIT database. Furthermore, 78 and 73 targets of calycosin 7-O-glucoside and notoginsenoside R1 were collected from the PharmMapper platform, respectively. After merging all the results and removing duplicate values, 141 active compounds and 854 targets of WPL were identified.

A total of 1645 GPL targets were screened from the GeneCards database, and 632 targets were further screened with relevance scores  $\geq 5$ .

### PPI network analysis

The Venny 2.1 tool was used to identify the common WPL and GPL targets, and 146 were retrieved (Fig. 1A). Then, 110 active compounds of WPL were identified using the 146 common targets. PPI network analysis was performed using the STRING database, with 146 common targets (Fig. 1B). The network consisted of 146 nodes and 3713 edges, and the average degree value was 50.9. CytoHubba, a Cytoscape plug-in, was used to select hub targets. The hub target network with ten nodes and 45 edges was visualised using Cytoscape software (Fig. 1C). The top ten hub targets were AKT1, PTGS2, TNF, CASP3, MAPK3, STAT3, HIF1A, TP53, IL6, and JUN.

### GO and KEGG enrichment analyses

We obtained 1759 GO items, including 72 molecular function (MF) items, 1627 biological process (BP) items, and 60 cellular components (CC) items, with screening criteria of  $P < 0.01$ . Figure 2A–C show the top 15 MF, BP, and CC items. The MF results suggested that WPL mainly focused on activating transcription factor binding, RNA polymerase II transcription factor binding, and hormone receptor binding. The BP items mainly included responses to oxidative stress, cellular responses to oxidative stress, and responses to reactive oxygen species (ROS). CC items mainly included membrane microdomains, membrane rafts, and vesicle lumens. KEGG enrichment analysis showed that anti-GPL WPL was mainly involved in 165 signalling pathways ( $P < 0.01$ ). The top 15 enriched pathways were the hypoxia-inducible factor (HIF)-1, IL-17, and NF- $\kappa$ B signalling pathways (Fig. 2D–E).

### Herb-compound-target (H-C-T) and target-pathway (T-P) network analysis

The H-C-T and T-P networks of WPL against GPLs were constructed using Cytoscape software (Fig. 3). The H-C-T network is composed of 266 nodes and 1469 edges. Herbs, compounds, and targets are represented by prisms, circles, and squares, respectively. In addition, the TP network includes 102 nodes and 308 edges. The targets and the top 15 KEGG pathways are represented by circles and squares, respectively. These networks suggest that WPL-treated GPLs involve multiple components, targets, and pathways.

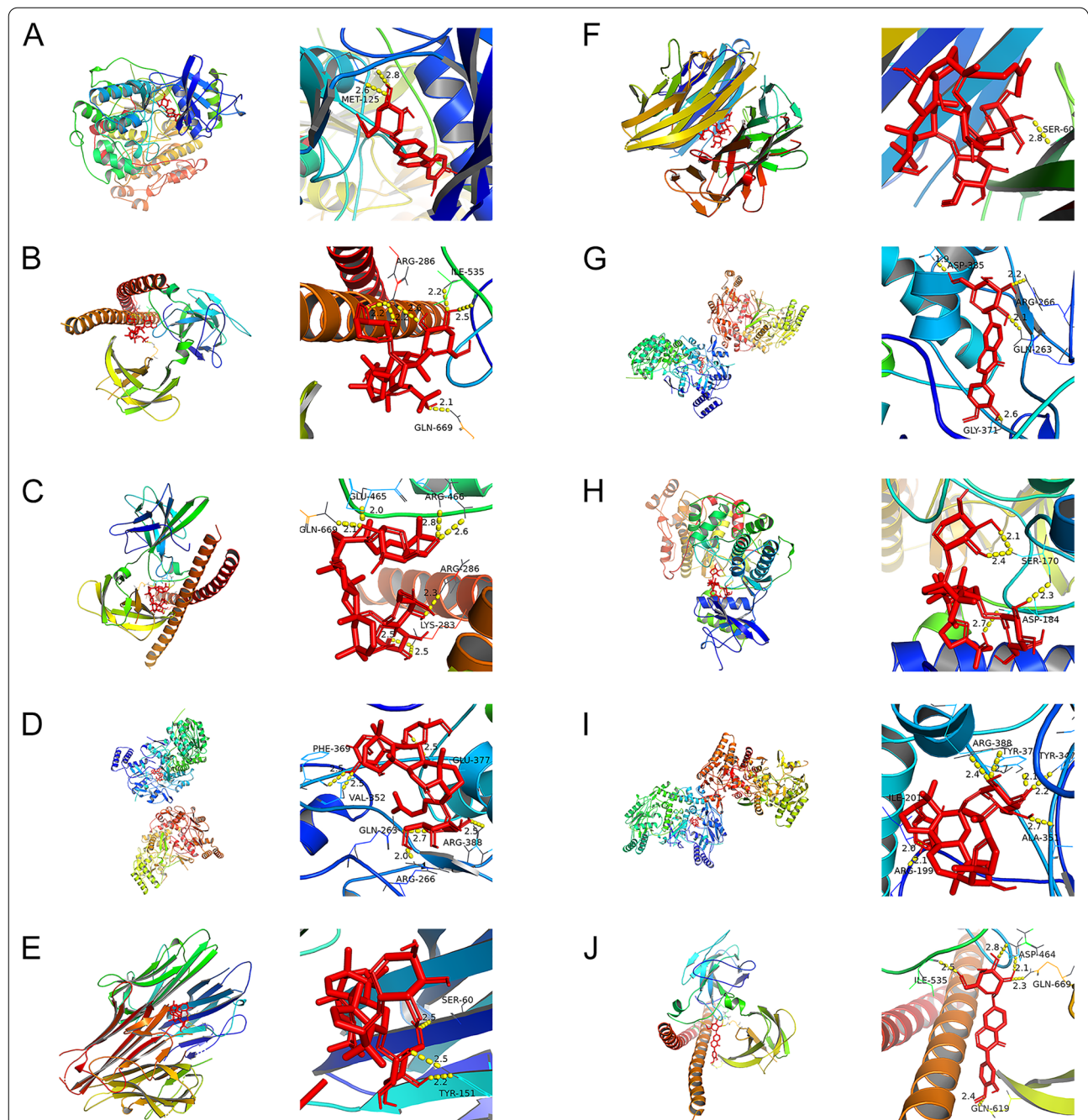
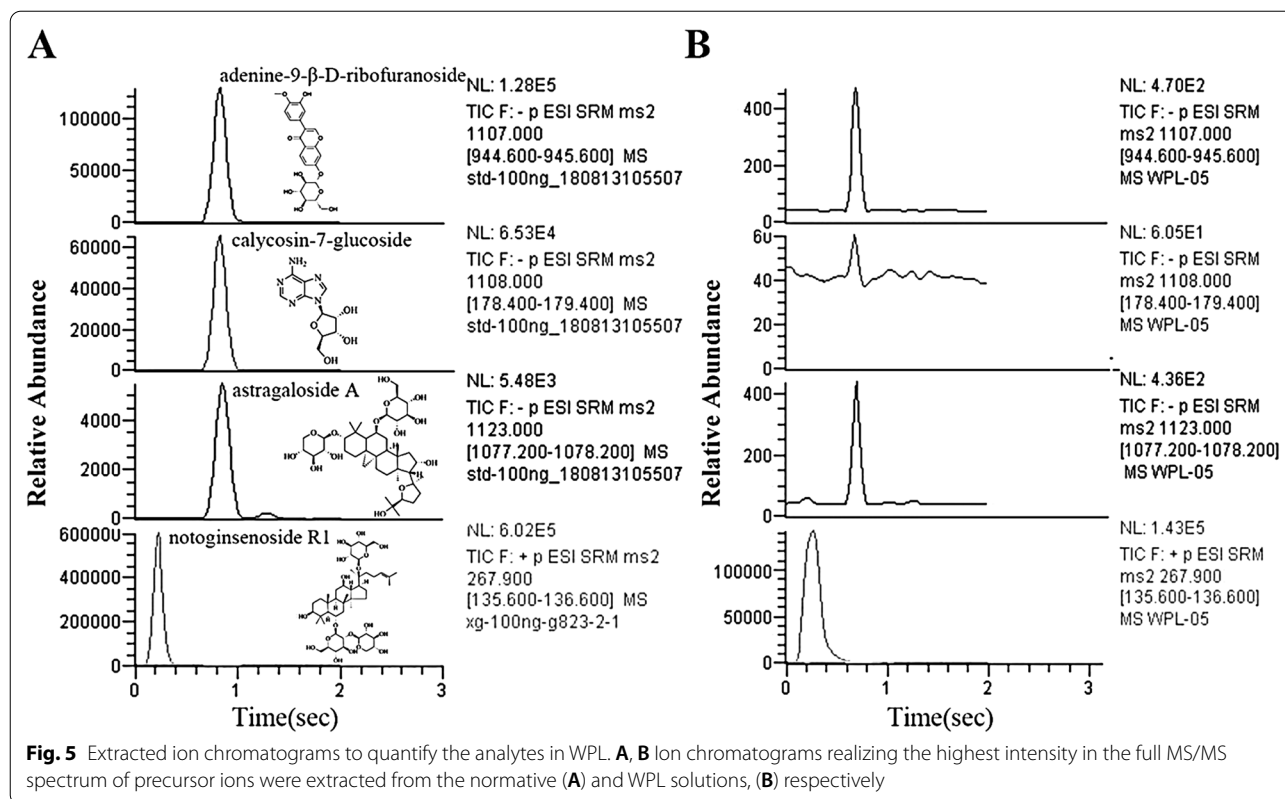


**Fig. 4** Docking of WPL-related active compounds and top hub genes. **A** Molecular docking of calycosin-7-O-β-D-glucoside and MAPK3, **B** astragaloside IV and JUN, **C** notoginsenoside R1 and JUN, **D** notoginsenoside R1 and NOS2, **E** astragaloside IV and TNF, **F** notoginsenoside R1 and TNF, **G** calycosin-7-O-β-D-glucoside and NOS2, **H** astragaloside IV and MAPK3, **I** astragaloside IV and NOS2, and **J** calycosin-7-O-β-D-glucoside and JUN

**Molecular docking analysis**

In our study, we docked seven hub targets (JUN, TNF, TP53, CASP3, MAPK3, NOS2, and BCL2) with four active compounds (calycosin-7-O-β-D-glucoside, astragaloside IV, notoginsenoside R1, and quinquefolan B) (Table 3) of WPL. Based on affinity <math>< -5 \text{ kcal/mol}</math>, we

obtained 27 pairs of docking results (Table 4). Moreover, calycosin-7-O-β-D-glucoside had a good binding ability with MAPK3 ( $-9.1 \text{ kcal/mol}$ ), NOS2 ( $-7.9 \text{ kcal/mol}$ ), and JUN ( $-7.5 \text{ kcal/mol}$ ). Astragaloside IV had a good binding ability with JUN ( $-8.7 \text{ kcal/mol}$ ), TNF



(−8.2 kcal/mol), MAPK3 (−7.7 kcal/mol), and NOS2 (−7.7 kcal/mol). Notoginsenoside R1 had a good binding ability with JUN (−8.2 kcal/mol), NOS2 (−8.2 kcal/mol), and TNF (−8 kcal/mol) (Fig. 4).

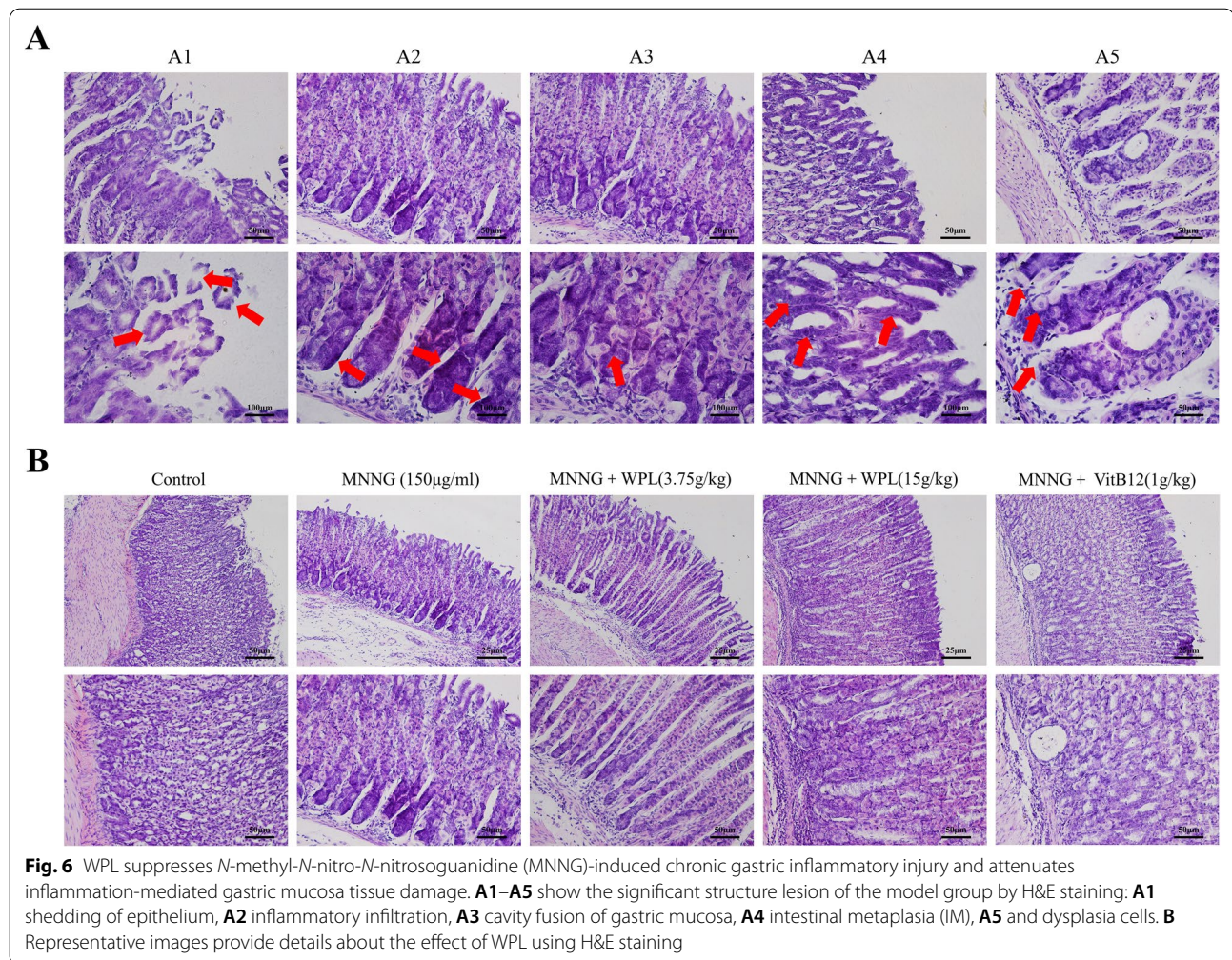
#### Quantitative analysis of the main components in WPL

The main components of WPL were determined by HPLC–MS analysis by matching the retention duration and mass spectra of the normative compounds with those of WPL. The retention duration and ion chromatograms were compared with those of the reference compounds to identify the main components of WPL, including notoginsenoside R1, calycosin-7-*O*-β-D-glucoside, astragaloside A, and adenine-9-β-D-ribofuranoside (Fig. 5, Table 5). Additionally, notoginsenoside R1, calycosin-7-*O*-β-D-glucoside, astragaloside A, and

adenine-9-β-D-ribofuranoside were detected at  $m/z$  929.0,  $m/z$  447.0,  $m/z$  785.0, and  $m/z$  267.9 at the  $[M+H]^+$  mode and at  $m/z$  324.8,  $m/z$  284.9,  $m/z$  324.9,  $m/z$  136.1 at the  $[M-H]^-$  mode, respectively, in high-resolution MS/MS configured with ESI (Table 5). Quantification was then performed by extracting the fragment ions with the highest intensity in the full MS spectra of the precursor ion (Fig. 5, Table 5). A standard calibration curve was used to determine the peak areas of the analytes. The calibration curves of all reference compounds displayed good linearity, which could be used to calculate the amount of each compound in WPL ( $r^2 \geq 0.9994$ , Table 2). Notoginsenoside R1 and calycosin-7-glucoside were the most abundant compounds (Table 2), indicating that these compounds should be regarded as chemical markers of WPL.

**Table 5** Retention time, precursor and quantitative ion  $m/z$ , normalized collision energy, and analyte content in WPL

Analyte	Retention time (s)	Precursor ion ( $m/z$ )	Quantitative fragment ( $m/z$ )	Normalized collision energy (NCE, %)	Content (mg/g)
Notoginsenoside R1	53	929.0	324.8	17	1.524
Adenine-9-β-D-ribofuranoside	14	267.9	136.1	17	0.448
Astragaloside A	51	785.0	324.9	9	0.139
Calycosin-7- <i>O</i> -β-D-glucoside	50	447.0	284.9	18	1.474



### WPL inhibits MNNG-induced chronic gastric inflammatory injury and attenuates inflammation-mediated gastric mucosa tissue damage

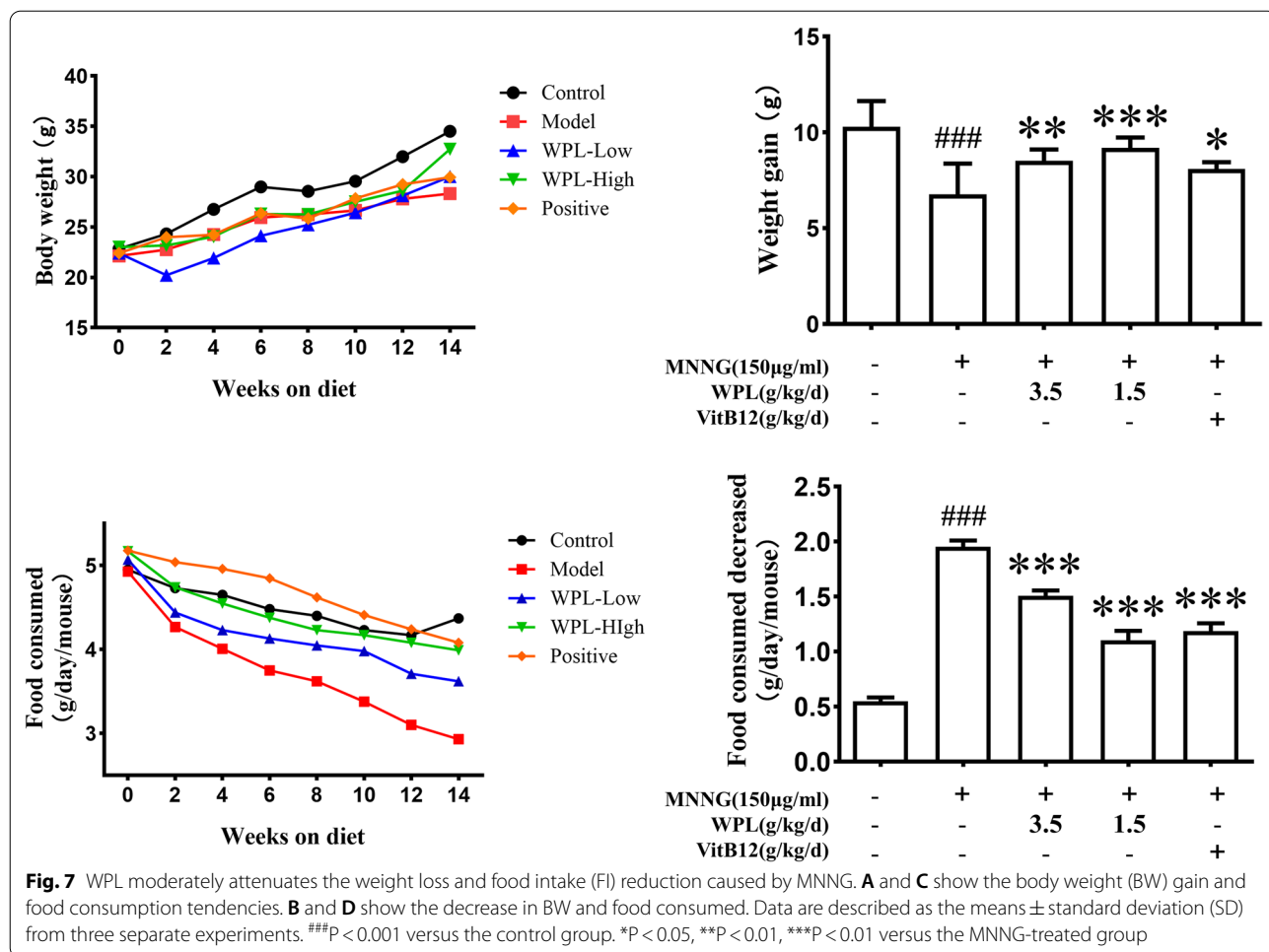
GPLs were induced using MNNG [43] to determine the anti-inflammatory role of WPL. Details regarding the effects of WPL were provided by H&E staining. According to Fig. 6A, the model group showed significant structural lesions of the gastric mucosa, such as epithelial shedding, and inflammatory infiltration. Likewise, epithelial cells exhibited vacuolation and cavity fusion in the gastric mucosa. Physaliphorous cells with a symmetrical thickness of the basement membrane were also visible. Dysplastic gastric epithelial cells were observed with enlarged, hyperchromatic, and crowded nuclei in the basement of the membrane (dysplasia). Furthermore, the irregular glands partially bifurcated or branched, indicating IM and dysplasia development. All these morphological changes suggested that apparent GPLs were present in the gastric mucosa (Fig. 6B). In contrast, the gastric mucosa in the WPL and VitB12 groups exhibited less

epithelial shedding, ulceration, and leukocyte infiltration. In addition, the gastric mucosa from the WPL group showed a more regular glandular cavity morphology and less or fewer enlarged, hyperchromatic, and crowded nuclei, indicating that WPL ameliorated the MNNG-induced gastric mucosal lesions.

Body weight (BW) and food intake (FI) were measured every 2 weeks to determine the gastric protective effects of WPL (Fig. 7). The BW gain rate and FI of the MNNG group mice significantly declined. However, administering WPL or VitB12 increased the BW and FI of mice, indicating that WPL and VitB12 moderately attenuated the weight loss and FI reduction caused by MNNG.

### WPL inhibits pro-inflammatory T helper 1 (Th1) cell infiltration to ameliorate gastric damage

IHC was performed to examine Th cell infiltration in inflammatory gastric mucosa tissues to uncover the pro-inflammatory effects of Th cells on GPL development.

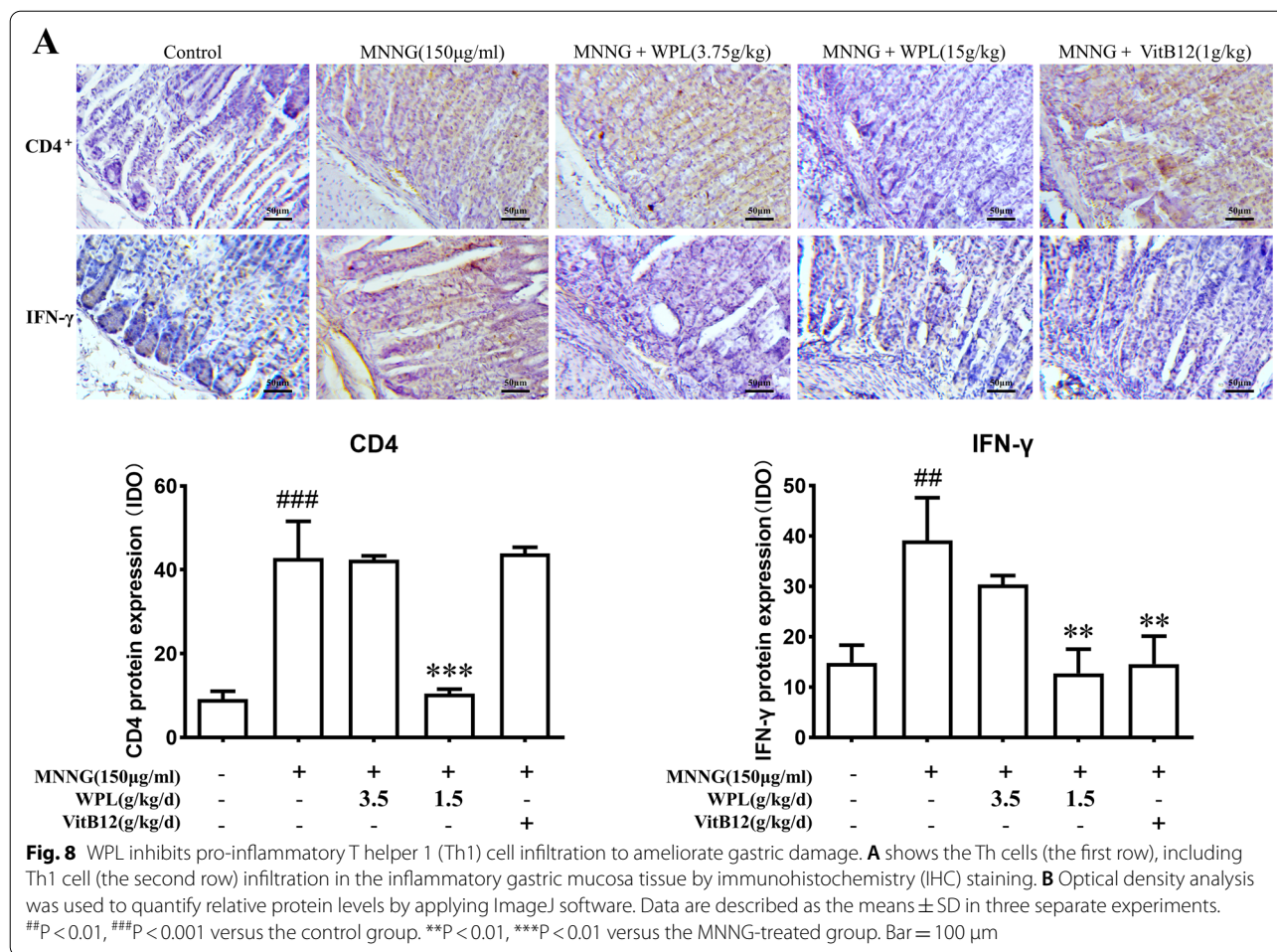


Abundant Th cell (CD4<sup>+</sup>) infiltration was observed after administering MNNG (Fig. 8A, first row). WPL and VitB12 inhibited Th cell infiltration, and a remarkable reduction was observed in the WPL group (*P* < 0.01). Among the Th cell subsets, Th1 (IFN-γ<sup>+</sup>) cells are pro-inflammatory factors that drive the growth of GPLs [9, 44, 45]. Based on the infiltration of total Th cells in the gastric mucosal tissues of the MNNG group (Fig. 8A, first row), the number of Th1 (IFN-γ<sup>+</sup>) cells significantly increased in the model group (Fig. 8A, second row, *P* < 0.01). Interestingly, both WPL and VitB12 suppressed excess pro-inflammatory Th1 cell infiltration (Fig. 8A, B) (*P* < 0.01).

**WPL decoction showed inhibitory effects on NF-κB signalling pathway and decreased pro-inflammatory enzymes and cytokine production in the gastric mucosa**

As the results of KEGG enrichment analysis, NF-κB signalling is critical for gastric inflammation and GPL development. Exposure to MNNG for 14 weeks

significantly enhanced NF-κB and IκBα phosphorylation. Nevertheless, MNNG-induced NF-κB and IκB-α phosphorylation was markedly reversed by the WPL pre-treatment (Fig. 9A–C). Compared with VitB12, WPL showed a comparable inhibitory effect on the NF-κB signalling pathway. Additionally, MNNG markedly induced transcriptional TNF-α and IL-6 upregulation, whereas WPL inhibited these effects (Fig. 9D, E), indicating that WPL can inhibit MNNG-induced inflammation in the gastric mucosa. Inflammatory stimuli can activate various enzymes, such as iNOS and COX-2, to promote inflammation. NF-κB signalling frequently induces NOX protein family members, such as NOX-2 and NOX-4, to complicate the inflammatory response by generating ROS. In our study, MNNG increased iNOS and COX-2 protein levels, whereas the WPL pre-treatment markedly decreased these protein levels (Fig. 10A–C). Furthermore, WPL attenuated MNNG-induced NOX2 and NOX4 protein upregulation (Fig. 10A, D, E). Therefore, WPL exerts



anti-inflammatory and gastric mucosa-protective effects by inhibiting NF-κB signalling and pro-inflammatory enzyme expression.

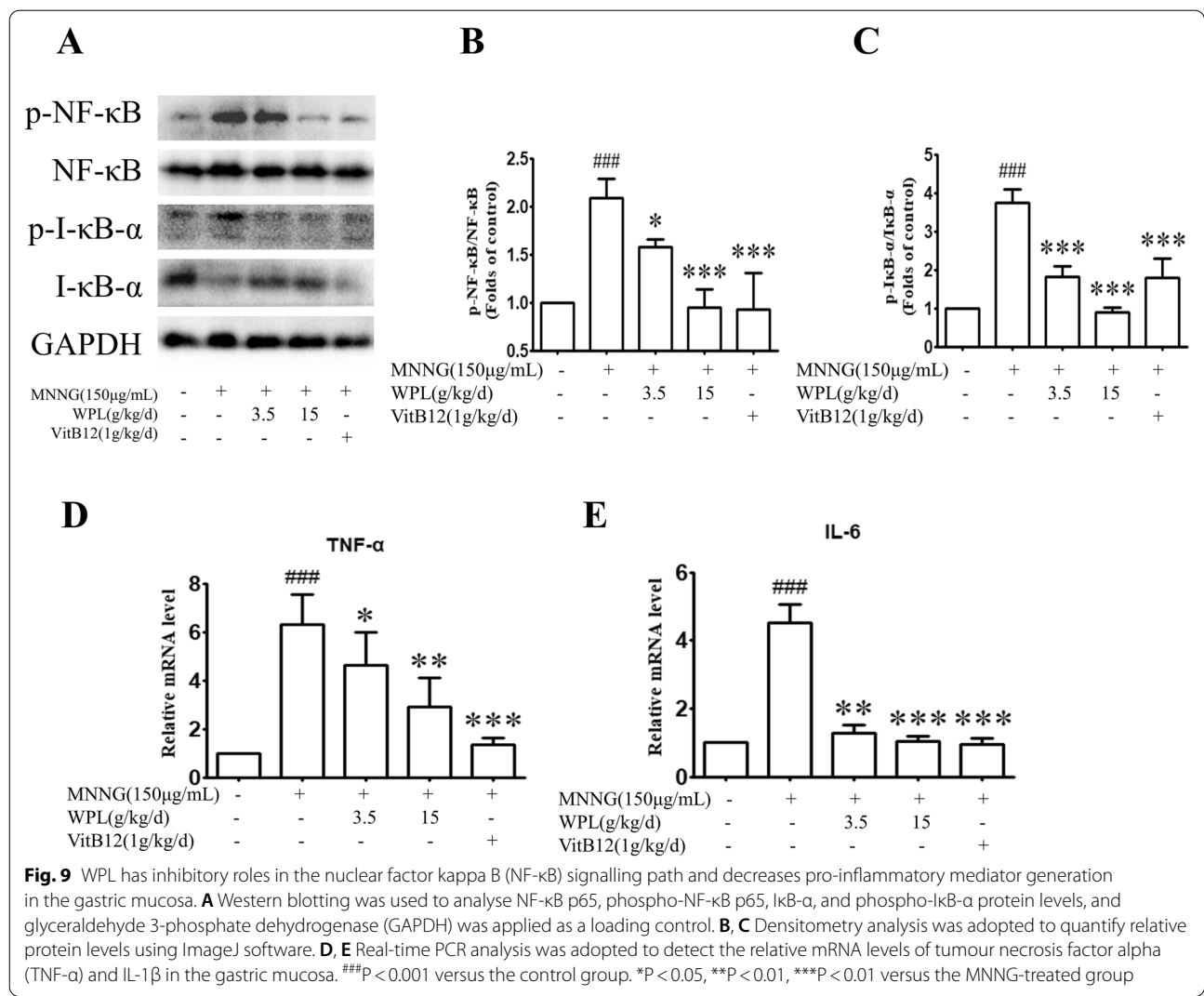
### Discussion

The poor outcome and mortality of GC can be prevented by early diagnosis and intervention at the GPL stage [46]. As a compound Chinese medicine and based on the theories of traditional Chinese medicine, WPL can ameliorate GPLs by enhancing the spleen, dispersing blood stasis, and detoxification. According to previous clinical trials, WPL has a great capacity to attenuate the clinical symptoms of GPLs [47]. In this study, network pharmacological analysis suggested that WPL relieves GPLs and may be associated with antioxidative stress and anti-inflammatory effects. An in vivo assay revealed that WPL attenuated MNNG-induced GPLs by inhibiting NF-κB pathway activation and pro-inflammatory Th1 cell infiltration in the gastric mucosa.

Here, we retrieved 110 active compounds and 146 potential targets of anti-GPL WPL from public databases and references. Notoginsenoside R1, calycosin-7-O-beta-D-glucoside,

astragaloside IV, and adenine-9-β-D-ribofuranoside were selected as chemical markers owing to their commercial value, high content, and pharmacological activity. HPLC-MS/MS results showed that notoginsenoside R1, with a content of 1.524 mg/g, was one of the most abundant compounds in WPL through quantitative analysis of the chemical markers. Notoginsenoside R1 exhibits pharmacological activities in alleviating oxidative stress, eliminating inflammation, and protecting damaged cells [7], suggesting that WPL extracts can be used to treat inflammatory diseases.

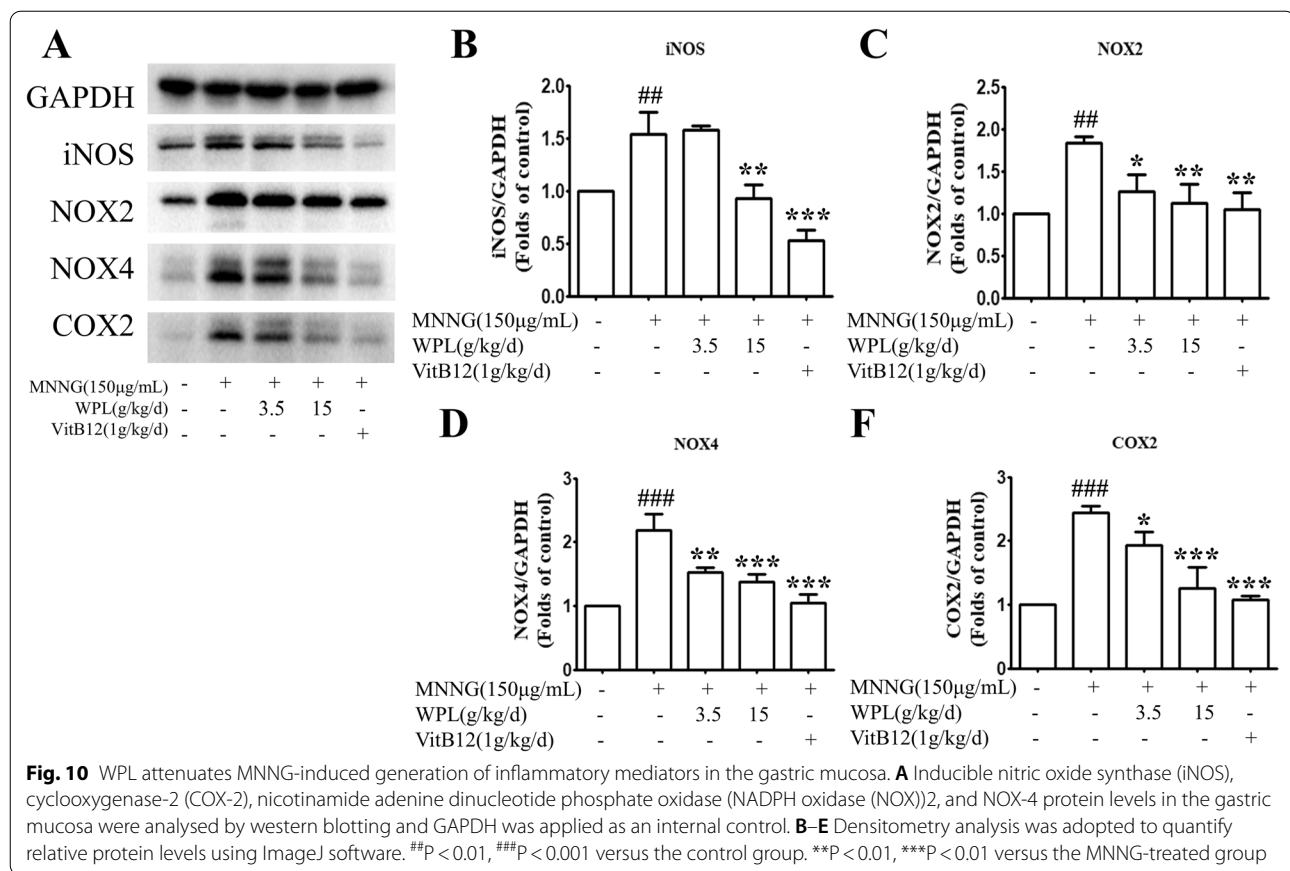
KEGG enrichment analysis showed that inflammation-related signalling pathways, including the HIF-1, IL-17, and NF-κB signalling pathways, were involved in anti-GPL WPL. GPL and GC development are related to continuous inflammation of the gastric mucosa, including NF-κB-mediated inflammation, the production of pro-inflammatory cytokines, and the infiltration of pro-inflammatory cells [48, 49]. Study suggests that NF-κB may promote tumorigenesis by regulating inflammation, cell proliferation, and apoptosis. And the activation of NF-κB contributes to GPL [50]. In our study, we found



that phosphorylation expression of NF-κB and IκB-α was upregulated in MNNG-induced GPL mice, which was weakened by WPL addition. Therefore, the traditional Chinese medicine, WPL, may serve as an inhibitor of the NF-κB pathway. For example, extracts from *Astragalus mongholicus Bunge* decreased angiogenesis-related molecules, such as vascular endothelial growth factor and COX-2, in ovarian tumor-bearing mice. Compounds extracted from *Atractylodes lancea (Thunb.) DC*, such as beta-eucalyptol and atractylone, can inhibit inflammation by blocking the NF-κB signalling pathway [20–22]. A previous study also demonstrated that the most effective ingredients of *Panax notoginseng (Burkill) F. H. Chen* had various pharmacological functions, such as anti-oxidative stress, anti-inflammatory, and anti-apoptotic effects [51, 52]. *Scleromitrion diffusum (Willd) R. J. Wang.* and *Hericium erinaceus (Bull.) Pers.* are commonly used to treat

gastrointestinal diseases, such as GC and CAG, by inhibiting tumour angiogenesis, proliferation, and apoptosis [24, 28–31]. Our previous study showed precancerous changes in the gastric mucosa in MNNG-induced GPL rats [7]. The most significant finding of this study was that WPL significantly attenuated MNNG-induced GPLs by inhibiting IκB/NF-κB pathway activation and pro-inflammatory Th1 cell infiltration in the gastric mucosa. The NF-κB signalling pathway is upstream of NOX2 and NOX4. NOX2 and NOX4 upregulation indicated ROS generation in MNNG-treated mice, and WPL reduced NOX2 and NOX4 levels. COX-2 and iNOS are downstream enzymes of the NF-κB pathway, and the products catalysed by these two enzymes are PEG2 and NO, which are further metabolised into ROS and RNS. An inhibitory effect of WPL was observed in this pathway. Moreover, cytokines and their function in recruiting





pro-inflammatory Th1 cells potentiate WPL's efficacy. WPL reversed the pro-inflammatory effects of Th1 cell infiltration and INF- $\gamma$  secretion. MNNG promoted TNF- $\alpha$  and IL-6 transcriptional levels, implying that the nuclear translocation of NF- $\kappa$ B is induced in the gastric mucosa. However, WPL exerted inhibitory effects on TNF- $\alpha$  and IL-6 transcription, suggesting that it may inhibit the nuclear translocation of NF- $\kappa$ B.

### Conclusion

In summary, the present study demonstrated that WPL inhibits MNNG-induced gastric inflammation and ameliorates inflammatory injury by suppressing the excess pro-inflammatory Th1 cell infiltration, inhibiting NF- $\kappa$ B signalling activation, and attenuating the expression of inflammatory enzymes in vivo. Our study provides evidence that WPL has a beneficial role in the intervention of GC formation and development. Unfortunately, our study also has shortcomings, such as WPL treatment of GPLs involves multiple pathways, we only validated NF- $\kappa$ B signalling pathway in animal study. Other mechanisms will be the focus of our follow-up study.

### Abbreviations

WPL: Weipiling; GPLs: Gastric precancerous lesions; HPLC-MS/MS: High-performance liquid chromatography with tandem mass spectrometry; MNNG: *N*-Methyl-*N*-nitro-*N*-nitrosoguanidine; H&E: Haematoxylin and eosin; Th1: T helper 1; INF- $\gamma$ : Interferon-gamma; IHC: Immunohistochemistry; NF- $\kappa$ B: Nuclear factor kappa B; RT-qPCR: Reverse transcription polymerase chain reaction; iNOS: Inducible nitric oxide synthase; COX-2: Cyclooxygenase-2; NADPH oxidase (NOX): Nicotinamide adenine dinucleotide phosphate oxidase; GC: Gastric cancer; CAG: Chronic atrophic gastritis; IM: Intestinal metaplasia; NOCs: *N*-Nitroso compounds; TCMID: Traditional Chinese Medicine Integrated Database; TCMSP: Traditional Chinese Medicine Systems Pharmacology Database and Analysis Platform; STITCH: Search Tool for Interacting Chemicals; QED: Quantitative estimate of drug-likeness; HIT: Herb Ingredients' Targets; PPI: Protein-protein interaction; GO: Gene Ontology; KEGG: Kyoto Encyclopaedia of Genes and Genomes; PDB: Protein Data Bank; VitB12: Vitamin B12; TCI: Tokyo Chemical Industry; HRP: Horseradish peroxidase; PRM: Parallel reaction monitoring; NCE: Normalised collision energies; PBS: Phosphate-buffered saline; DAB: Diaminobenzidine; RIPA: Radioimmunoprecipitation assay; BCA: Bicinchoninic acid; SDS-PAGE: Sodium dodecyl-sulphate polyacrylamide gel electrophoresis; PVDF: Polyvinylidene fluoride; BSA: Bovine serum albumin; TBST: Tris-buffered saline and Tween 20; cDNA: Complementary DNA; TNF- $\alpha$ : Tumour necrosis factor alpha; SD: Standard deviation; MF: Molecular function; BP: Biological process; CC: Cellular components; ROS: Reactive oxygen species; HIF: Hypoxia-inducible factor; BW: Body weight; FI: Food intake.

### Acknowledgements

Not applicable.

### Author contributions

The study was designed by SYL, HFP; the experiments were conducted by PHY, HMY, HLZ, SFW, QYL and SYL; data were analyzed by PHY, HLZ, QYL, SFW and SYL; the manuscript was written by PHY, HLZ, QYL, SYL and YQL; the manuscript was reviewed by PHY, HMY, HLZ, QYL, SFW, YY, QW, YQL, HFP and SYL. All authors read and approved the final manuscript.

### Funding

This work was supported by National Natural Science Foundation of China [Grant number 82174319]; Natural Science Foundation of Guangdong province [Grant number 2019A1515010822] and [Grant number 2021A1515110932]; China Postdoctoral Science Foundation [Grant number 2022M710030]; Key-Area Research and Development Program of Guangdong Province [Grant number 2020B1111100011]; and Guangdong Provincial Key Laboratory of TCM Pathogenesis and Prescriptions of Heart and Spleen Diseases [grant number 2022B1212010012].

### Availability of data and materials

The datasets used and/or analysed during the current study are available from the corresponding author on reasonable request.

### Declarations

#### Ethics approval and consent to participate

This study was approved by the Institutional Animal Care and Use Committee of Guangzhou University of Traditional Chinese Medicine.

#### Consent for publication

Not applicable.

#### Competing interests

The authors declare that they have no competing interests.

#### Author details

<sup>1</sup>Science and Technology Innovation Center, Guangzhou University of Chinese Medicine, Guangzhou 510405, China. <sup>2</sup>Department of Emergency Ward, The First Affiliated Hospital of Guizhou University of Chinese Medicine, Guiyang 550001, China. <sup>3</sup>Department of Gastroenterology, The Second Affiliated Hospital of Guangzhou University of Chinese Medicine, Guangzhou 510405, China. <sup>4</sup>Guangzhou University of Chinese Medicine, Guangzhou 510405, China. <sup>5</sup>Research Center of Chinese Herbal Resources Science and Engineering, School of Pharmaceutical Sciences, Guangzhou University of Chinese Medicine, Guangzhou 510405, China. <sup>6</sup>Joint Laboratory for Translational Cancer Research of Chinese Medicine of the Ministry of Education of the People's Republic of China, Guangzhou 510405, China. <sup>7</sup>International Institute for Translational Chinese Medicine, Guangzhou University of Chinese Medicine, Guangzhou 510405, China. <sup>8</sup>Dongguan Institute of Guangzhou University of Chinese Medicine, Dongguan 523808, China.

Received: 1 August 2022 Accepted: 29 August 2022

Published online: 09 September 2022

### References

- Corso S, Giordano S. How can gastric cancer molecular profiling guide future therapies? *Trends Mol Med*. 2016;22(7):534–44.
- Smyth EC, Nilsson M, Grabsch HI, van Grieken NC, Lordick F. Gastric cancer. *Lancet (Lond, Engl)*. 2020;396(10251):635–48.
- Cheng XJ, Lin JC, Tu SP. Etiology and prevention of gastric cancer. *Gastrointest Tumors*. 2016;3(1):25–36.
- Siegel RL, Miller KD, Fuchs HE, Jemal A. Cancer statistics, 2022. *CA Cancer J Clin*. 2022;72(1):7–33.
- Katai H, Ishikawa T, Akazawa K, Isobe Y, Miyashiro I, Oda I, et al. Five-year survival analysis of surgically resected gastric cancer cases in Japan: a retrospective analysis of more than 100,000 patients from the nationwide registry of the Japanese Gastric Cancer Association (2001–2007). *Gastric Cancer*. 2018;21(1):144–54.
- You WC, Zhang L, Gail MH, Li JY, Chang YS, Blot WJ, et al. Precancerous lesions in two counties of China with contrasting gastric cancer risk. *Int J Epidemiol*. 1998;27(6):945–8.
- Cai T, Zhang C, Zeng X, Zhao Z, Yan Y, Yu X, et al. Protective effects of Weipixiao decoction against MNNG-induced gastric precancerous lesions in rats. *Biomed Pharmacother*. 2019;120:109427.
- Liu W, Zhao ZM, Liu YL, Pan HF, Lin LZ. Weipiling ameliorates gastric precancerous lesions in Atp4a(-/-) mice. *BMC Complement Altern Med*. 2019;19(1):318.
- Fox JG, Wang TC. Inflammation, atrophy, and gastric cancer. *J Clin Invest*. 2007;117(1):60–9.
- Hartgrink HH, Jansen EP, van Grieken NC, van de Velde CJ. Gastric cancer. *Lancet*. 2009;374(9688):477–90.
- Cutsem EV, Sagaert X, Topal B, Haustermans K, Prenen H. Gastric cancer. *Lancet*. 2016;388:2654–64.
- Tricker AR, Preussmann R. Carcinogenic N-nitrosamines in the diet: occurrence, formation, mechanisms and carcinogenic potential. *Mutat Res*. 1991;259(3–4):277–89.
- Wyatt MD, Pittman DL. Methylating agents and DNA repair responses: methylated bases and sources of strand breaks. *Chem Res Toxicol*. 2006;19(12):1580–94.
- Isyraqiah F, Kutty MK, Durairajanayagam D, Singh HJ. Leptin enhances N-methyl-N'-nitro-N-nitrosoguanidine (MNNG)-induced tumour growth in gastric mucosa of male Sprague-Dawley rats. *Mol Biol Rep*. 2019;46(6):5967–75.
- Raphael KR, Sabu M, Kumar KH, Kuttan R. Inhibition of N-Methyl N'-nitro-N-nitrosoguanidine (MNNG) induced gastric carcinogenesis by *Phyllanthus amarus* extract. *Asian Pac J Cancer Prev*. 2006;7(2):299–302.
- Van Hecke T, Vanden Bussche J, Vanhaecke L, Vossen E, Van Camp J, De Smet S. Nitrite curing of chicken, pork, and beef inhibits oxidation but does not affect N-nitroso compound (NOC)-specific DNA adduct formation during in vitro digestion. *J Agric Food Chem*. 2014;62(8):1980–8.
- Fahrer J, Kaina B. Impact of DNA repair on the dose-response of colorectal cancer formation induced by dietary carcinogens. *Food Chem Toxicol*. 2017;106(Pt B):583–94.
- Osaki LH, Bockerstett KA, Wong CF, Ford EL, Madison BB, DiPaolo RJ, et al. Interferon- $\gamma$  directly induces gastric epithelial cell death and is required for progression to metaplasia. *J Pathol*. 2019;247(4):513–23.
- Zeng J, Pan H, Zhao Z, Gong D, Liu W, Cai T, et al. Clinical effect of Jianpi Huayu Jiedu compound prescription on gastric precancerous lesions and its influence on the expression of HIF-1 $\alpha$  and VEGF. *Lishizhen Tradit Chin Med*. 2018;29:1544–8.
- Yin G, Tang D, Dai J, Liu M, Wu M, Sun YU, et al. Combination efficacy of astragalus membranaceus and Curcuma wenyujin at different stages of tumor progression in an imageable orthotopic nude mouse model of metastatic human ovarian cancer expressing red fluorescent protein. *Anticancer Res*. 2015;35(6):3193–207.
- Yu C, Xiong Y, Chen D, Li Y, Xu B, Lin Y, et al. Ameliorative effects of atracylodin on intestinal inflammation and co-occurring dysmotility in both constipation and diarrhea prominent rats. *Korean J Physiol Pharmacol*. 2017;21(1):1–9.
- Moon PD, Han NR, Lee JS, Kim HY, Hong S, Kim HJ, et al.  $\beta$ -eudesmol inhibits thymic stromal lymphopoietin through blockade of caspase-1/NF- $\kappa$ B signal cascade in allergic rhinitis murine model. *Chem Biol Interact*. 2018;294:101–6.
- Liu Z, Liu M, Liu M, Li J. Methylanthraquinone from *Hedyotis diffusa* Willd induces Ca(2+)-mediated apoptosis in human breast cancer cells. *Toxicol In Vitro*. 2010;24(1):142–7.
- Abdulla MA, Fard AA, Sabaratnam V, Wong KH, Kuppusamy UR, Abdullah N, et al. Potential activity of aqueous extract of culinary-medicinal Lion's Mane mushroom, *Hericium erinaceus* (Bull.: Fr) Pers. (Aphyllophoromycetideae) in accelerating wound healing in rats. *Int J Med Mushrooms*. 2011;13(1):33–9.
- Lin J, Wei L, Shen A, Cai Q, Xu W, Li H, et al. *Hedyotis diffusa* Willd extract suppresses Sonic hedgehog signaling leading to the inhibition of colorectal cancer angiogenesis. *Int J Oncol*. 2013;42(2):651–6.
- Niu Y, Meng QX. Chemical and preclinical studies on *Hedyotis diffusa* with anticancer potential. *J Asian Nat Prod Res*. 2013;15(5):550–65.

27. Wang M, Gao Y, Xu D, Gao Q. A polysaccharide from cultured mycelium of *Hericium erinaceus* and its anti-chronic atrophic gastritis activity. *Int J Biol Macromol*. 2015;81:656–61.
28. Wang C, Zhou X, Wang Y, Wei D, Deng C, Xu X, et al. The antitumor constituents from *Hedyotis diffusa* Willd. *Molecules* (Basel, Switzerland). 2017;22(12):2101.
29. Ren Z, Qin T, Liu X, Luo Y, Qiu F, Long Y, et al. Optimization of *Hericium erinaceus* polysaccharide-loaded Poly (lactic-co-glycolic acid) nanoparticles by RSM and its absorption in Caco-2 cell monolayers. *Int J Biol Macromol*. 2018;118(Pt A):932–7.
30. Wang XY, Yin JY, Zhao MM, Liu SY, Nie SP, Xie MY. Gastroprotective activity of polysaccharide from *Hericium erinaceus* against ethanol-induced gastric mucosal lesion and pylorus ligation-induced gastric ulcer, and its antioxidant activities. *Carbohydr Polym*. 2018;186:100–9.
31. Wang XY, Zhang DD, Yin JY, Nie SP, Xie MY. Recent developments in *Hericium erinaceus* polysaccharides: extraction, purification, structural characteristics and biological activities. *Crit Rev Food Sci Nutr*. 2019;59(sup1):S96-s115.
32. Zhang L, Han L, Wang X, Wei Y, Zheng J, Zhao L, et al. Exploring the mechanisms underlying the therapeutic effect of *Salvia miltiorrhiza* in diabetic nephropathy using network pharmacology and molecular docking. *Biosci Rep*. 2021;41(6).
33. Huang L, Xie D, Yu Y, Liu H, Shi Y, Shi T, et al. TCMID 2.0: a comprehensive resource for TCM. *Nucleic Acids Res*. 2018;46(D1):D1117-d20.
34. Ru J, Li P, Wang J, Zhou W, Li B, Huang C, et al. TCMSP: a database of systems pharmacology for drug discovery from herbal medicines. *J Cheminform*. 2014;6:13.
35. Szklarczyk D, Santos A, von Mering C, Jensen LJ, Bork P, Kuhn M. STITCH 5: augmenting protein-chemical interaction networks with tissue and affinity data. *Nucleic Acids Res*. 2016;44(D1):D380–4.
36. Bickerton GR, Paolini GV, Besnard J, Muresan S, Hopkins AL. Quantifying the chemical beauty of drugs. *Nat Chem*. 2012;4(2):90–8.
37. Liang X, Li H, Li S. A novel network pharmacology approach to analyse traditional herbal formulae: the Liu-Wei-Di-Huang pill as a case study. *Mol Biosyst*. 2014;10(5):1014–22.
38. Ye H, Ye L, Kang H, Zhang D, Tao L, Tang K, et al. HIT: linking herbal active ingredients to targets. *Nucleic Acids Res*. 2011;39(Database issue):D1055–9.
39. Sterling T, Irwin JJ. ZINC 15—ligand discovery for everyone. *J Chem Inf Model*. 2015;55(11):2324–37.
40. Burley SK, Berman HM, Kleywegt GJ, Markley JL, Nakamura H, Velankar S. Protein Data Bank (PDB): the single global macromolecular structure archive. *Methods Mol Biol* (Clifton, NJ). 2017;1607:627–41.
41. Trott O, Olson AJ. AutoDock Vina: improving the speed and accuracy of docking with a new scoring function, efficient optimization, and multi-threading. *J Comput Chem*. 2010;31(2):455–61.
42. Seeliger D, de Groot BL. Ligand docking and binding site analysis with PyMOL and Autodock/Vina. *J Comput Aided Mol Des*. 2010;24(5):417–22.
43. Huang L, Qi DJ, He W, Xu AM. Omeprazole promotes carcinogenesis of fore-stomach in mice with co-stimulation of nitrosamine. *Oncotarget*. 2017;8(41):70332–44.
44. Peek RM Jr, Crabtree JE. Helicobacter infection and gastric neoplasia. *J Pathol*. 2006;208(2):233–48.
45. Nguyen TL, Khurana SS, Bellone CJ, Capoccia BJ, Sagartz JE, Kesman RA Jr, et al. Autoimmune gastritis mediated by CD4+ T cells promotes the development of gastric cancer. *Cancer Res*. 2013;73(7):2117–26.
46. Chen TH, Chiu CT, Lee C, Chu YY, Cheng HT, Hsu JT, et al. Circulating microRNA-22-3p predicts the malignant progression of precancerous gastric lesions from intestinal metaplasia to early adenocarcinoma. *Dig Dis Sci*. 2018;63(9):2301–8.
47. Guo YL, Jing R, Pan HF, Fang J. Effect of the treatment of Jianpi Huayu Jiedu for patients with chronic atrophic gastritis and its influence on cyclin E protein expression. *Chin J Exp Tradit Med Form*. 2013;19:292–5.
48. Tye H, Jenkins BJ. Tying the knot between cytokine and toll-like receptor signaling in gastrointestinal tract cancers. *Cancer Sci*. 2013;104(9):1139–45.
49. Gambhir S, Vyas D, Hollis M, Aekka A, Vyas A. Nuclear factor kappa B role in inflammation associated gastrointestinal malignancies. *World J Gastroenterol*. 2015;21(11):3174–83.
50. Xu J, Shen W, Pei B, Wang X, Sun D, Li Y, et al. Xiao Tan He Wei Decoction reverses MNNG-induced precancerous lesions of gastric carcinoma in vivo and vitro: regulation of apoptosis through NF- $\kappa$ B pathway. *Biomed Pharmacother*. 2018;108:95–102.
51. Xu D, Huang P, Yu Z, Xing DH, Ouyang S, Xing G. Efficacy and safety of *Panax notoginseng* saponin therapy for acute intracerebral hemorrhage, meta-analysis, and mini review of potential mechanisms of action. *Front Neurol*. 2014;5:274.
52. Hu S, Liu T, Wu Y, Yang W, Hu S, Sun Z, et al. Panax notoginseng saponins suppress lipopolysaccharide-induced barrier disruption and monocyte adhesion on bEnd.3 cells via the opposite modulation of Nrf2 antioxidant and NF- $\kappa$ B inflammatory pathways. *Phytother Res*. 2019;33(12):3163–76.

## Publisher's Note

Springer Nature remains neutral with regard to jurisdictional claims in published maps and institutional affiliations.

### Ready to submit your research? Choose BMC and benefit from:

- fast, convenient online submission
- thorough peer review by experienced researchers in your field
- rapid publication on acceptance
- support for research data, including large and complex data types
- gold Open Access which fosters wider collaboration and increased citations
- maximum visibility for your research: over 100M website views per year

At BMC, research is always in progress.

Learn more [biomedcentral.com/submissions](https://biomedcentral.com/submissions)

